J Seismol (2018) 22:69–81
DOI 10.1007/s10950-017-9692-y

ORIGINAL ARTICLE

BARENTS16: a 1-D velocity model for the western Barents Sea

Myrto Pirli · Johannes Schweitzer

Received: 20 March 2017 / Accepted: 17 August 2017 / Published online: 25 August 2017

Abstract A minimum 1-D seismic velocity model for routine seismic event location purposes was determined for the area of the western Barents Sea, using a modified version of the VELEST code. The resulting model, BARENTS16, and corresponding station corrections were produced using data from stations at regional distances, the vast majority located in the periphery of the recorded seismic activity, due to the unfavorable land–sea distribution. Recorded seismicity is approached through the listings of a joint bulletin, resulting from the merging of several international and regional bulletins for the region, as well as additional parametric data from temporary deployments. We discuss the challenges posed by this extreme network-seismicity geometry in terms of velocity estimation resolution and result stability. Although the conditions do not facilitate the estimation of meaningful station corrections at the farthermost stations, and even well-resolved corrections do not have a convincing contribution, we show that the process can still converge to a stable velocity average for the crust and upper mantle, in good agreement with a priori information about the regional structure and geology, which reduces adequately errors in event location estimates.

M. Pirli (✉) · J. Schweitzer
NORSAR, P.O. Box 53, 2027 Kjeller, Norway
e-mail: myrto.pirli@gmail.com

J. Schweitzer
CEED, University of Oslo, P.O. Box 1028, Blindern, 0315 Oslo, Norway

Keywords Barents Sea · European Arctic · Minimum 1-D model · Station corrections · Relocation

1 Introduction

The epicontinental Barents Sea, located in the European Arctic, is a region of low deformation, with limited seismicity (Fig. 1a). Tectonic earthquake activity is observed mostly at its margins, in particular in the Svalbard Archipelago, and along the Senja Fracture Zone (SFZ) that delineates the continent–ocean boundary to the southwest. To the north of the SFZ, a thick sedimentary wedge (Czuba et al. 2011) spreads across the passive continental margin separating the Barents shelf from the North Atlantic mid-ocean-ridge system that accommodates most of the seismic activity in the wider region. Although rare, earthquakes on the Barents shelf are observed, as e.g., at its southwestern part, an area characterized by the succession of Cretaceous basins and highs (e.g., Smelror et al. 2009). This area, as well as its immediate vicinity to the East, hosts significant hydrocarbon exploration-related activity, with potential for intensification, a fact that leads to increased interest in regional neotectonics and small magnitude seismicity.

The seismic network in the region is rather sparse, its geometry restricted by the geographic distribution of land. The only permanent seismic station located in the center of the region is the single, 3-component (3C) station BJO1 on Bjørnøya (Bear Island), whereas all

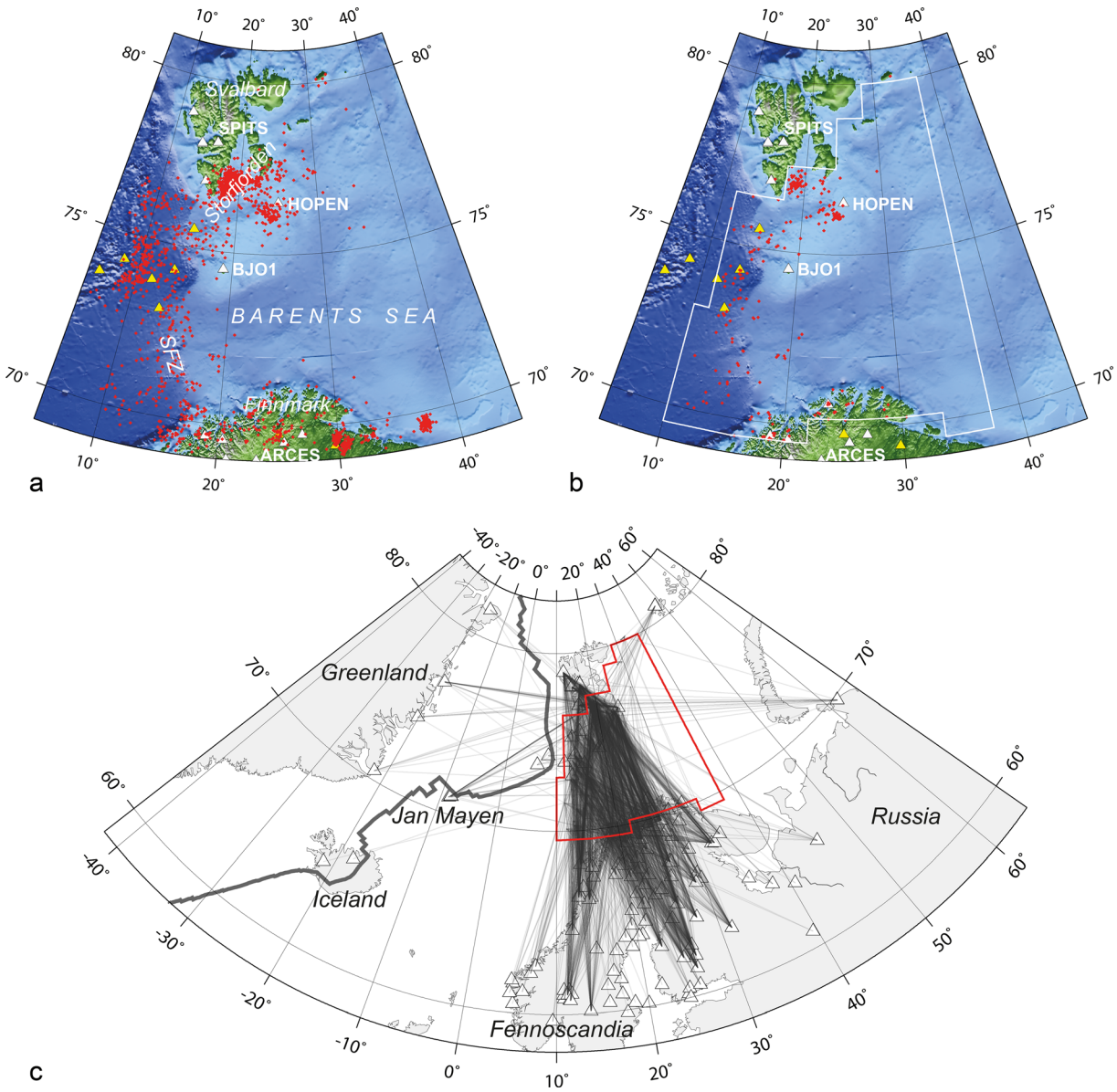

Fig. 1 **a** Map of the central-western Barents Sea region. Stations of the permanent, international seismic network are shown as white triangles, whereas temporary seismic stations as yellow triangles. Epicenters of events located by more than three stations in the unified bulletin employed herein are noted as red points. **b** Same as **a**, but only the 245 events selected as input to the inversion algorithm VELEST are shown. The corresponding study region is noted as a white polygon. **c** Map of the wider European Arctic region, showing the seismic stations (white triangles) used to locate the 245 events of the input dataset and the achieved ray coverage (thin, gray lines). The study region is enclosed in the red polygon, and the plate boundary (i.e., mid-ocean ridge system) is noted with the thick gray line

the rest are deployed in the periphery, mostly in Finnmark at the southern side and Svalbard in the North. Apart from Jan Mayen, stations to the West and East can be found only at far regional distances, on Greenland and Russia, and can only provide adequate quality recordings for larger magnitude events. Thus, routine seismic monitoring in the Barents Sea region is mainly based on the regional network of seismic arrays (i.e., Apatity, ARCES, FINES, HFS, NOA, NORES, SPITS) in Fennoscandia and Svalbard. Larger event locations are supplemented with phase readings on single, 3C stations.

However, the highly variable crustal structure in the wider Barents Sea region, with extremely thick crust in Fennoscandia (Moho depth between 40 and 60 km, e.g., Grad et al. 2009; Silvennoinen et al. 2014), shallower Moho in the Barents shelf (24–35 km in the western part, e.g., Grad et al. 2009; Hauser et al. 2011; Klitzke et al. 2015; Ritzmann et al. 2007), and slightly deeper crust on Svalbard (26–36 km, e.g., Grad et al. 2009; Hauser et al. 2011; Ritzmann et al. 2007; Wilde-Piórko 2015), introduces complications in routine event location. For routine seismic location purposes, where the usage of 3-D or multiple 1-D velocity models is not standard, a proper, average model for the Barents Sea that covers adequately the regional stations generally employed has been missing. NORSAR uses a seismic velocity model developed for Fennoscandia (Mykkeltveit and Ringdal 1981) for its routine locations of regional seismicity, while the BAREY and BAREZ 1-D velocity models (Hicks et al. 2004; Schweitzer and Kennett 2007) and local/regional 1-D averages extracted from available 3-D models (e.g., local average for Storfjorden, Svalbard in Pirli et al. 2010) have been found to perform reasonably, but with problems to properly model event-station paths that include the Barents shelf. We address this problematic by determining a new, average, 1-D velocity model for the western Barents Sea, using the minimum 1-D model approach (Kissling 1988; Kissling et al. 1994). In addition, we assess the validity and utility in terms of improvement to location estimates of the associated station corrections for the international, regional network typically used to locate seismicity in the region.

2 Data and methods

To calculate the minimum 1-D model, we used the VELEST code, following Kissling et al. (1994). The algorithm inverts as input onset times of P and S phases and station information, as well as a starting seismic velocity structure and hypocenters of the events, to determine an average model where seismic velocities inside the layers are an approximation of the best velocity average, weighted by the total ray length inside the layer and station corrections that are the weighted average station delays for the total of observations for each station (e.g., Kissling 1988; Kissling et al. 1994; Haslinger 1998). As onset time information, the program can only utilize the first arriving P and S phases, secondary onsets not being supported by the built-in ray-tracer. For our application, this program package needed to be modified. In a first step, the Earth flattening approximation (Müller 1977) was implemented to calculate correctly seismic travel times over large distances in crustal and upper mantle models. In addition, several formatting changes for input and output parameters were needed to handle e.g., longer station codes and model dimensions of more than 1000 km. A description of the datasets and procedure employed herein follows in the next sections.

2.1 Input hypocenters

Since the Barents Sea region is a low seismicity area with increased activity levels observed at its periphery, and to ensure an adequate amount of well-located data for the calculation of the minimum 1-D model, we resorted to a joint bulletin compiled within the frame of a joint Norwegian–Russian project (Schweitzer et al. 2017), focusing here on the wider area of the western Barents Sea, for the time interval 1990–February 2016. The joint catalog was constructed by merging the following available bulletins for the European Arctic region:

- Reviewed International Seismological Centre Bulletin (ISC 2014), 1990–March 31, 2013
- Non-reviewed ISC Bulletin (ISC 2014), April 1, 2013–February 2016
- Reviewed Bulletins of the Experimental International Data Center (EIDC) and the Preliminary International Data Center (PIDC) in Arlington, Virginia, and the International Data Centre in Vienna, Austria, 1996–December 2000
- NORSAR Regional Reviewed Bulletin (1990–1998: unpublished; 1998–February 2016: NORSAR REB, http://www.norsardata.no/NDC/bulletins/regional/)
- Bulletin of the Norwegian National Seismic Network (University of Bergen, ftp://ftp.geo.uib.no/pub/seismo/DATA/PARAMETRIC/CAT/)
- Helsinki Seismic Bulletin (http://www.helsinki.fi/geo/seismo/english/bulletins/), 1991–2014
- Bulletin of the Arkhangelsk Seismic Network (http://www.iepn.ru), 2004–2015

In addition, parametric data from the following stations, projects and temporary deployments were included:

- The International Polar Year 2007–2008 (IPY) project "The Dynamic Continental Margin" (e.g., Schweitzer 2011), involving several events on the sedimentary wedge between Bjørnøya and the mid-ocean ridge system (Pirli et al. 2011), September 2007–October 2008
- Events from the Storfjorden, Svalbard, aftershock sequence (Pirli et al. 2013), February 2008–July 2012
- A collection of ground truth (GT) events used to develop attenuation relations (Hicks et al. 2004) and a 3-D model for the Barents Sea (Hauser et al. 2011), 1990–2010
- A collection of phase readings from events in northern Norway, April 1991–August 2015 and events in the European Arctic from Greenland stations, 1998–2015 (Steven Gibbons, pers. comm.)
- A collection of phase readings from station AMD of the Kola Regional Seismological Centre, May 1995–March 2004 (Andrey Fedorov, pers. comm.)
- A collection of phase readings from the temporary stations installed in Finland within the frame of the ScanArray initiative (Thybo et al. 2012), October 2013–May 2015 (Ilma Janutyté, pers. comm.)

Due to different readings being reported for the same onsets by different sources, multiple entries needed to be eliminated. This was achieved by calculating a mean onset time for each phase reading and adding the observed spread in onset time to the reading uncertainty.

In this study, we use only a subset of this newly compiled bulletin and concentrate on the region enclosed in the polygon of Fig. 1b. The resulting joint bulletin, containing more than 4000 events in the study polygon, was homogenized through relocation with algorithm HYPOSAT (Schweitzer 2001), using the BAREY velocity model (Schweitzer and Kennett 2007). The relocation allowed the identification of wrongly merged events both in the original sources and in the final joint bulletin which were corrected whenever possible, otherwise removed. Unsurprisingly, the constant development of the recording networks leads to much improved location estimates during the last decade compared to the situation earlier in the compiled bulletin (a discussion about such developments, focusing on Svalbard, can be found, e.g., in Pirli et al. 2013).

Since the Storfjorden earthquake series lies outside the main focus of this study, only locations with more than 10 observing stations were included in the input dataset for the calculation of the minimum 1-D model, instead of the hundreds of located events associated with this activity (Pirli et al. 2013; Junek et al. 2014). Further, we removed all stations at epicentral distances larger than 15° and discarded location results obtained with less than four stations and with an azimuthal gap larger than 200°. The study region does not include the mining areas in Finnmark and on the Kola Peninsula.

Resolution for focal depth determination strongly depends on the geometry of the recording network and in particular the distance between the nearest station and the events (e.g., Havskov et al. 2012), as well as the rather sparse regional network in the study region cannot resolve event focal depths, as e.g., demonstrated for seismicity in the vicinity of Hopen Island (Stange and Schweitzer 2004); to overcome this problem, we located each event with the focal depth fixed at 2, 5, 10, 15, and 20 km and chose a best solution in each case, in terms of number of well-fitting defining observations and residual levels, which we included in our input dataset. After selecting only those events with a minimum of 10 observations, we obtained a quite small dataset for the size of the study region, consisting of 245 earthquakes (Fig. 1b). This dataset includes 3633 first P- and 2614 first S-readings, consistent with VELEST requirement that only first onsets are used. The corresponding ray-paths are displayed in Fig. 1c, where it becomes evident that there is no coverage for the eastern part of the study region, while stations in the far periphery of the employed geometry (i.e., on Greenland, Iceland, Russia, and southern Sweden) are represented with only a few ray-paths that cover a limited azimuthal range.

2.2 Input velocity models

We tested a large number of starting velocity models, the majority representative for the Barents Sea, but also models describing regions of significantly diverse lithospheric structure. Among the typical Barents Sea models are BAREY and BAREZ (Schweitzer and Kennett 2007), as well as averages

from the three-dimensional model Barents3D (Levshin et al. 2007; Ritzmann et al. 2007; www.norsar.no/seismology/barents3d) from which we extracted overall and regionalized averages for the Barents Sea and surrounding regions. Some of the latter (e.g., models describing the crustal and upper mantle structure in Fennoscandia or the oceanic crust west of the SFZ) are among the extreme models that were tested, together with model NOES by Morozov et al. (2015). The velocity models were then expanded to a succession of 2- to 3-km-thick layers in the upper crust, 5-km-thick layers in the lower crust, and a couple of layers in the upper mantle, down to 150 km, typically in cascades of 9 to 15 layers.

2.3 Inversion for the minimum 1-D model

VELEST requires a station to be assigned as a reference, so that station corrections are calculated in relation to it (Kissling 1995). Although not located centrally in the study region, the ARCES array was the best choice to be assigned reference station status, since it offers good temporal, azimuthal, and distance range coverage, while providing data of good signal-to-noise ratio, without too many timing problems, at least in recent years. We did test, however, unsuccessfully, station BJO1 on Bjørnøya that is positioned ideally in the center of the study region, and the SPITS array on Spitsbergen (Fig. 1a).

Several tests were performed variating the damping factors for the hypocentral, seismic velocity, and station correction information. Since there is no resolution for focal depth determination, we adjusted the damping factor for the focal depth to avoid variations larger than about 5 km. The most stable results with meaningful variations of velocity values during inversion were obtained with the following combination of damping factors for the origin time, horizontal coordinates, focal depth, seismic velocity, and station corrections, respectively: othet = xythet = 0.01, zthet = 5.0, vthet = 1.0, and stathet = 0.1 (see Kissling 1995).

Tests with initially fixed S-velocities and/or station corrections did not produce stable results, so we inverted for both Vp, Vs, and station corrections from start. Typically, nine iterations were enough to converge to a stable model geometry when approaching a minimum; we prolonged, however, the inversion procedure for all promising results to ensure that velocities were no longer fluctuating. Once this was achieved, we tested various depths for the major discontinuities and boundaries within the employed depth range, first determining the Moho, then the Conrad discontinuity and finally any other layer boundaries.

Inversion results were evaluated in terms of RMS (Fig. 2a) and variance reduction for the specified number of iterations. They were further compared on the basis of overall and iteration-specific hypocenter shifts, selecting those models that displayed a smoothly decaying curve, without increases during later iterations (Fig. 2b). Another deciding factor was the number of rays crossing each model layer to ascertain adequate resolution. Finally, the distribution of station corrections was taken into account favoring solutions that produced the largest amount of physically meaningful values (see Sect. 3.1).

Solutions that produced strong RMS minima and stable velocity structure were then assessed in terms of their agreement with a priori information on Earth structure in the region, the corresponding agreement of the geographic distribution of station corrections, through hypocenter-shift tests, and by taking into account the quality of the results when relocating the dataset (see Sect. 3.2).

3 Results and discussion

3.1 Minimum 1-D model

In total, more than 150 different starting model and parameter setting combinations were tested. Starting models with large numbers of layers soon collapsed to simpler geometries with two layers in the crust and two layers in the upper mantle, reflecting the restrictions imposed by the input dataset. Employed events have their hypocenters largely between 5 and 15 km, with only a small number of events at 2 and 20 km depth (gray bars in Fig. 3). In addition, the distances of the stations from the recorded seismicity favor the observation of regional phases (about 93% of the considered phases are Pn/Sn phases) that do not provide resolution for the shallower layers.

When the model space was adequately explored for each starting model (e.g., ranges of extremely low to extremely high velocities were used for each layer-geometry), the best fitting Moho was first established, followed by similar tests for the Conrad discontinuity and the layering in the upper mantle. The best fitting Moho depth converged to 36 km, both for solutions with

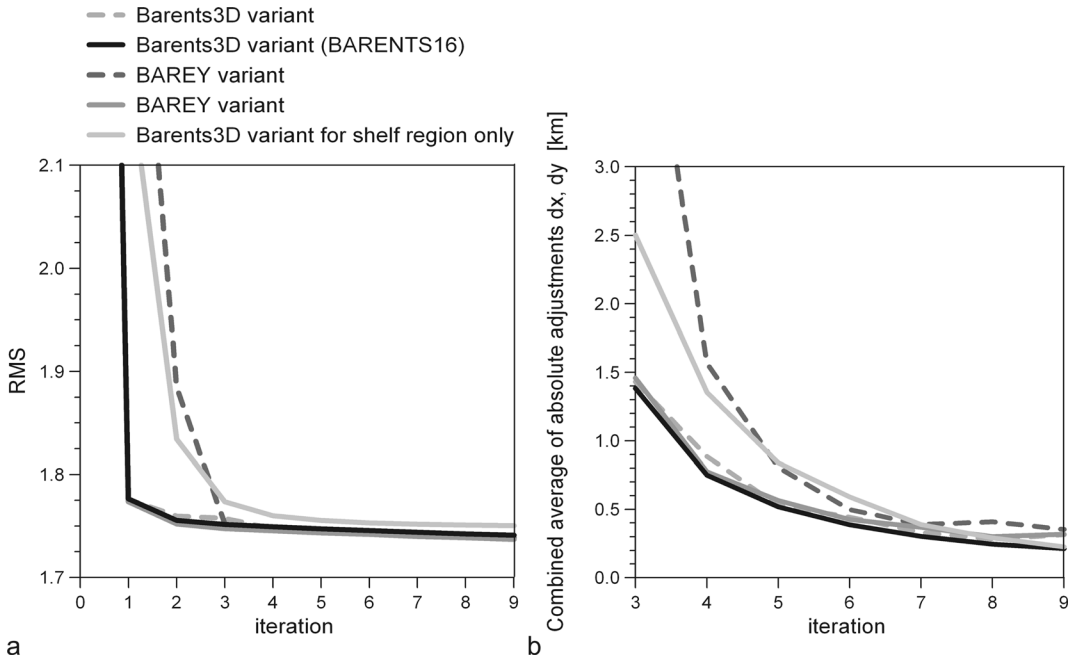

Fig. 2 **a** Curve of the RMS variation in the course of nine iterations for the best performing models obtained in this study. The RMS-axis is clipped to the value of 2.1 to facilitate observation. **b** Curve of the variation of the combined (vector) epicenter adjustments in kilometers, in the *x* and *y* directions for the same models as in **a**. The first iterations are omitted to facilitate observation

starting models based on BAREY/BAREZ and on averages extracted from Barents3D. This is a quite shallower Moho compared to the 41 km of BAREY, which was the model used to initially locate the input dataset. It is however deeper than the average Moho depth for the Barents shelf (32.5 km) according to Barents3D, but comparable with Barents3D averages (34–35.5 km) for the Cretaceous volcanic province E–SE of Svalbard and the Olga Basin and Sentralbanken High areas (for a structural map of the Barents Sea, see Smelror et al. 2009). It is also in good agreement with the crustal thickness of 35 km obtained by Klitzke et al. (2015) for the shelf region.

Since our stations span an altitude range between about 1 km above sea level and 2.6 km below (i.e., stations on Greenland and IPY project OBS deployment, respectively), we tested model geometries with an additional shallow crustal layer that would contain all stations. However, the scarcity of hypocenters in this depth range resulted in anomalously high Vp/Vs ratios and a failure to reach a stable velocity result for this layer, even though some metrics, e.g., RMS reduction and hypocentral shifts, suggested a promising outcome.

To test the stability of the most promising results, we randomly shifted the obtained epicenters by 15 km in the horizontal plane. Since the focal depth is kept under control during the inversion, we did not incorporate shifts in the vertical dimension. Again, all tested models performed similarly, showing only minor variations in seismic velocities and station corrections, while shifted event epicenters returned very close to their original locations. The few outliers that occurred in some cases could be accounted for by poorly constrained initial location estimates attributed to the geometry of the recording network.

The best fitting model, referred to hereafter as BARENTS16, is presented in Table 1 (including the standard deviation for seismic velocities) and Fig. 3. It is a variant of the overall Barents3D average for the study region (pink line in Fig. 3), with the Conrad discontinuity at 20 km and the second upper mantle layer at 75 km depth (red line in Fig. 3). Upper crust velocities are lower than those of BAREY (black line in Fig. 3), but comparable to those of global model AK135 (Kennett et al. 1995; gray line in Fig. 3), whereas seismic velocities in the lower crust are significantly lower than both. They are however higher than the corresponding ones in several other well-performing results herein. The observed effect can be best understood when taking into account the focal depth

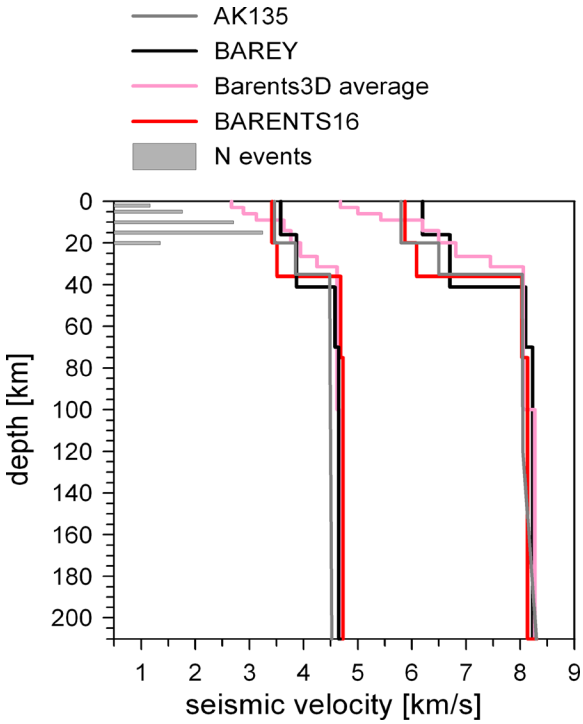

Fig. 3 1-D P (right) and S (left) velocity Earth structure as described by models AK135 (gray), BAREY (black), the 1-D average extracted for the western Barents Sea from the Barents3D model (pink), and the best-fitting model, BARENTS16, calculated in this study. The depth axis accommodates in addition a bar chart (gray bars) showing number of events with focal depth. Twenty-one events have their source at 2 km, 40 at 5 km, 70 at 10 km, 87 at 15 km, and 27 at 20 km depth

distribution of the earthquakes in the employed dataset; the gray bars in Fig. 3 show that there are no hypocenters in the lower crust, and although there exist ray-paths passing through this medium, the resolution is limited. Therefore, what is eventually achieved is an average between the low velocities in the shallow sedimentary layers and the higher velocities just above the Moho (the extent of the values is demonstrated by the 1-D average

Table 1 Obtained 1-D model BARENTS16 for the western Barents Sea region

Depth (km)	Vp (km/s)	Vs (km/s)
0	5.87 ± 0.060	3.42 ± 0.025
20	6.09 ± 0.100	3.51 ± 0.046
36	8.03 ± 0.035	4.69 ± 0.016
75	8.14 ± 0.008	4.73 ± 0.005
210	8.30 (fixed)	4.72 (fixed)

model extracted from Barents3D for the study region, shown in pink in Fig. 3). The obtained model has slightly slower Vp values in the upper mantle than BAREY, but faster Vs values, which are noticeably higher (+ 2.4%) just below the Moho.

Our best model estimates exhibit very similar patterns when considering the geographic distribution of the obtained station corrections. Noticeable differences are observed though for the median of the obtained values (not shown). The overall range of calculated station corrections for the best fitting model is presented in the histograms of Fig. 4a, b. The majority of stations exhibit negative corrections for P-phases and positive for S-phases, although extreme absolute values are mostly negative. Station corrections for a minimum 1-D model express to a large extent the heterogeneity in the 3-D regional seismic velocity structure, as well as the effect of local near-surface velocities, and as such, it is their relative differences that are important. However, large, absolute values have no physical meaning (e.g., Haslinger 1998). The challenge in the current application is twofold: (i) we employ a rather extreme geometry between recording stations, seismicity and the medium we wish to sample and establish its structure, and (ii) several of the employed stations, although contributing to stabilizing individual earthquake location estimates, do not achieve adequate coverage of the study region in terms of azimuth or distance and cannot provide a meaningful average.

Figure 4c shows the distribution of the P and S station corrections shown in Fig. 4a, b with number of observations. There is a clear correlation between large absolute station-correction values and small amounts of data per station per phase-type, while the levels are generally lower for P- than for S-phase corrections. Taking jointly into account the distributions of Fig. 4, we consider station corrections larger than ± 4 s as meaningless and exclude them from all subsequent discussion. To expand some more on point (i) above, there exist ray-paths in our data scheme (see Fig. 1c) that sample highly heterogeneous media, as for example, in the case of stations west of the mid-ocean ridge that contain the effect of the oceanic crust as well as that of the structure at the point of emergence. No meaningful averages can be obtained for such stations either, so we ignore all associated results. BARENTS16 is the model with the largest number of resolvable station corrections (not shown).

The geographic distribution of the station corrections we interpret is mapped in Fig. 5a,b with value

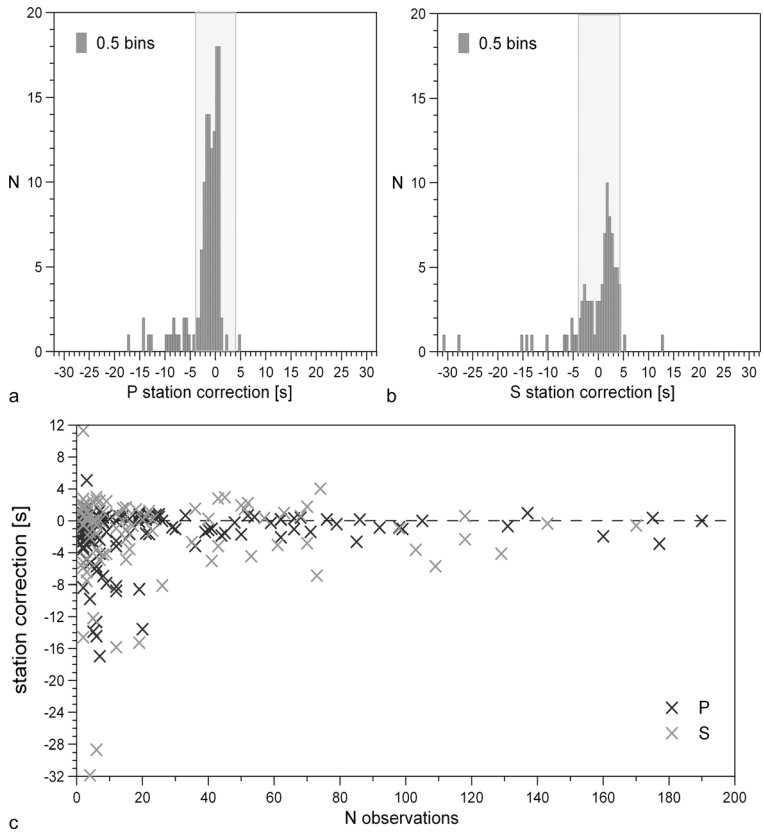

Fig. 4 Histograms of the station corrections in increments of 0.5 s for the best fitting model. The range of meaningful correction values is marked with a gray rectangle. **a** For the P-phase station corrections. **b** For the S-phase station corrections. **c** Distribution of the obtained station corrections for the best fitting model against number of observations for each station

ranges translated into the color scale shown therein. Stations for which corrections could not be calculated due to insufficient amount of data are not shown. Stations with corrections that have no physical meaning are shown in black. Such cases are observed at the geographic limits of the network, as well as among the IPY OBS deployment west of Bjørnøya (black triangles in Fig. 5a,b). The latter exhibits a divide between negative and positive corrections that largely follows the continent–ocean boundary in the region (e.g., Czuba et al. 2011). Regarding the distribution in Fennoscandia, most corrections reflect the levels of absolute P- and S-travel time residuals presented for the Scandinavian Mountain region by Hejrani et al. (2017), while their distribution is also similar, but seems to be more controlled by the geographic extent of the Archaean basement for the P-delays (e.g., Eken et al. 2007, 2008). However, the sign of the residuals is inverted; although at first hand this appears problematic, the following points need to be taken jointly into account: (i) The reference stations used in our study and Hejrani et al. (2017) are different; they use the Hagfors array (HFS), situated in southern Sweden on the Proterozoic Sveconorwegian domain, whereas ARCES that is used as reference station, herein, is deployed on the Archaean basement. As demonstrated by, e.g., Eken et al. (2007), although the thickness of the crust at the regions of these two stations is comparable, the southern location (Hagfors region) has a thicker lower crust of higher velocity compared to the upper crust that dominates the Archaean basement. (ii) The medium sampled predominantly in the present study is the crust in its entirety and the upper mantle, with a dominance of Pn phase readings whose paths have variable lengths in the faster upper mantle, depending on the depth of the Moho. ARCES and stations on the Baltic Shield are located on thicker crust than, e.g., stations on the Caledonide basement (e.g., Grad et al. 2009), so rays with longer parts in the faster medium travel predominantly with higher velocities that dominate the average values reflected by the station corrections (average horizontal ray length in the upper mantle is ~ 750 km, against only ~ 50 km vertical length). Thus, herein, it is the average velocity

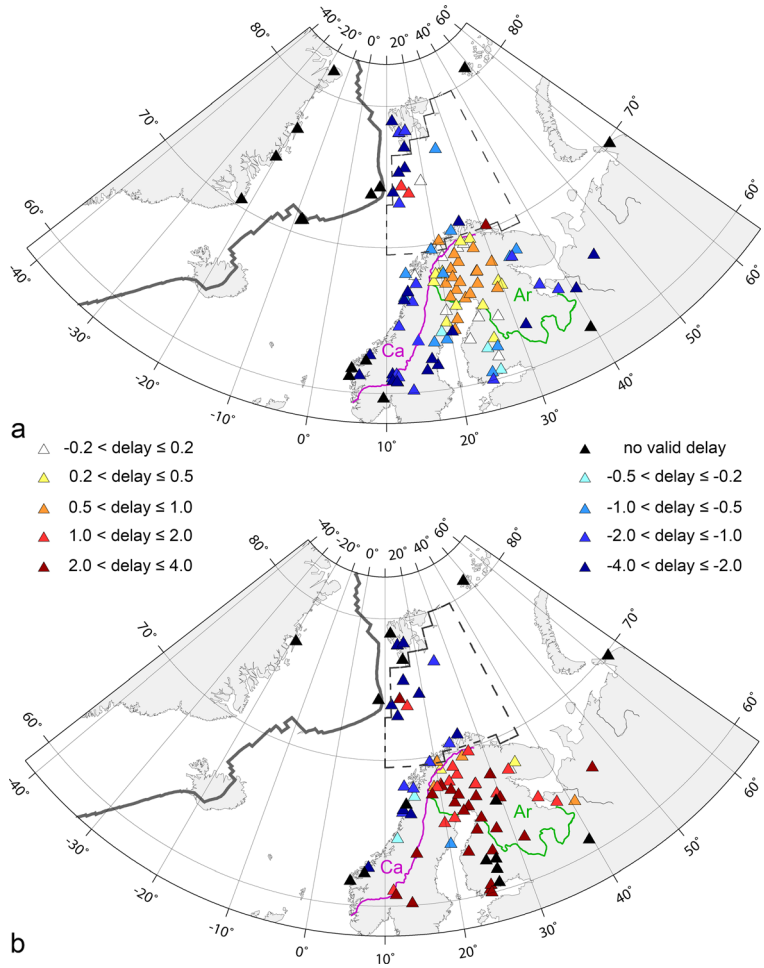

Fig. 5 Map of the station delays (s) for model BARENTS16. Resolvable values are depicted applying the color scale shown in the figure, while stations without meaningful values are mapped with black triangles. Stations with too few data to calculate corrections are not mapped at all. The plate boundary is drawn with a bold gray line; the boundaries of the Caledonian (Ca) and Archaean (Ar) basement on Fennoscandia (Eken et al. 2008) in magenta and green, respectively; and the study area is enclosed in a dashed polygon. **a** Distribution for P-waves. **b** Distribution for S-waves

structure relative to that at the reference station that is mostly reflected in the station correction values rather than the near-surface structure, which dominates the results of Hejrani et al. (2017). This is accentuated by the fact that our stations lay predominantly outside the medium whose structure we wish to resolve. What this means in practical terms for using the calculated station corrections will be discussed in Sect. 3.2.

3.2 Input dataset relocation

To test the stability of the obtained BARENTS16 model, we relocated the input dataset using HYPOSAT. To this purpose, we now used all available onset-time readings, contrary to the input dataset to the inversion algorithm that requires only first onsets, as well as travel time differences, ignoring any available backazimuth and slowness observations. This amounted to a total of 7370 input observations for the 245 events. The following relocation runs were performed:

A. Using the BAREY 1-D velocity model (Schweitzer and Kennett 2007) that was used to produce the start solutions
B. Using the BARENTS16 model without station corrections
C. Using the BARENTS16 model with station corrections, but only for reasonably resolved values
D. Using the BARENTS16 model with reasonably resolved station corrections, but applied only to first onset phases, to simulate the VELEST inversion settings

Figure 6 summarizes and compares the results of these four runs in terms of achieved location accuracy. Box and whisker plots (Tukey 1977) are employed to

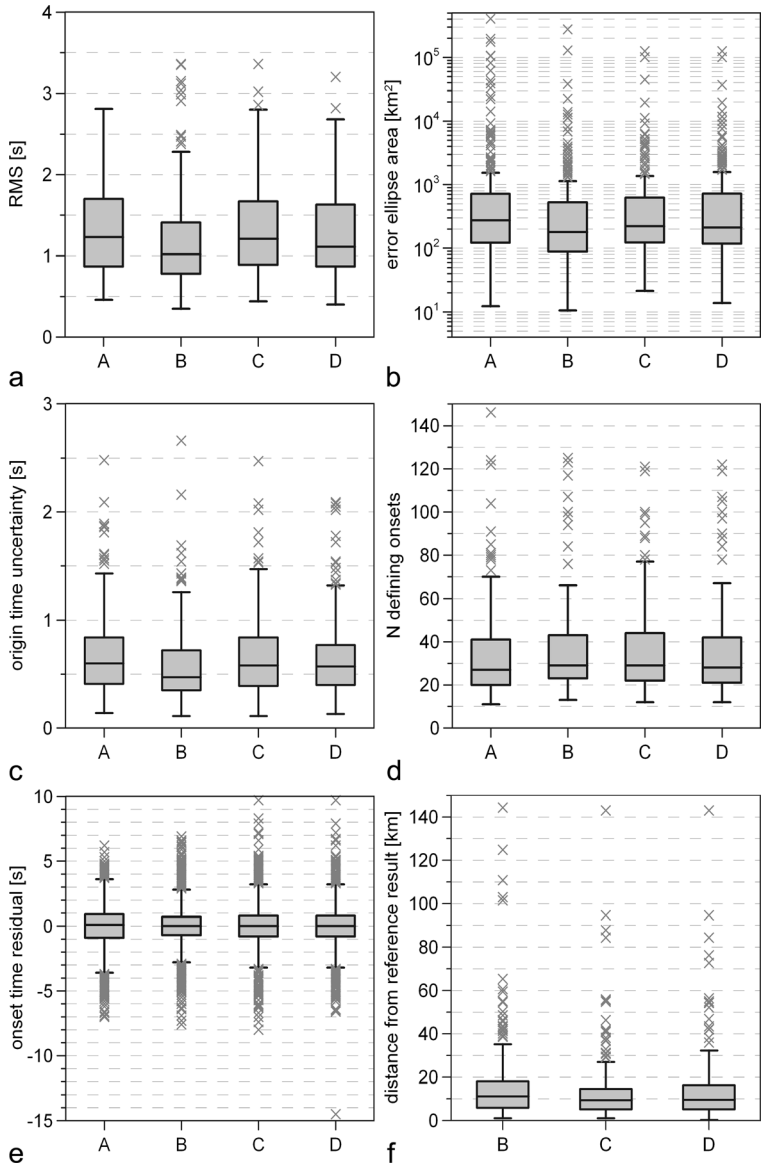

Fig. 6 Box and whisker plots for various metrics characterizing the event location results of event relocation runs A, B, C, and D, performed using BAREY, BARENTS16 without station corrections, BARENTS16 with all resolvable station corrections, and BARENTS16 with station corrections only for first onsets, respectively. **a** For RMS of location estimate. **b** For the area of the 95% confidence-level error ellipse. **c** For the uncertainty in origin time estimation. **d** For the number of defining onsets used per location estimate. **e** For the time residual of defining onsets. **f** For the distance between relocation results for combinations B, C, D and the BAREY model (A) for the 245 events used as VELEST input

describe and compare the distributions of these populations. Each gray box represents the interquartile range (IQR) of the distribution, the bottom noting the first quartile (Q1), the top the third (Q3), and the black line the second (Q2), which corresponds to the median of the distribution. Whiskers denote the values within the range Q1 – 1.5 × IQR and Q3 + 1.5 × IQR, whereas values outside that range are defined as outliers (crosses).

BARENTS16 without station corrections (B) shows a distribution of events with significantly lower RMS values than any other combination (Fig. 6a), whereas BAREY (A) and BARENTS16 with station corrections (C) perform very similarly; improvement (i.e., median RMS reduction) compared to the reference model (A) is ~ 17% for (B), 2% for (C), and 10% for (D). BARENTS16 with station corrections for first onsets only (D) performs slightly better than C but does not approach the improvement achieved by usage without station corrections. Similar observations can be made regarding the area of the 95% confidence level error-ellipse (Fig. 6b), with a ~ 35% median improvement for (B) against ~ 19% for (C) and ~ 23% for (D); the uncertainty in the event origin time estimate (Fig. 6c),

with ~ 22% median improvement for (B) against ~ 3% for (C) and 5% for (D); and the time residuals of the onsets actually used by the location algorithm to define each solution (Fig. 6e), with zero-median distributions for (B), (C) and (D), (B) exhibiting the narrowest range. Overall, the distributions for combination B are not only better concerning the median values of these location uncertainty metrics, but also in terms of the maximum spread of each distribution, outliers commencing at lower values compared to the three other cases. In particular, the significant improvement exhibited in the case of onset-time residuals between A and B increases our confidence in the obtained model. It is worth noting at this point that overall, the dataset relocation with the new average model in any combination (B, C, D) would employ a larger number of onsets as defining observations than BAREY (A 5157, B 5537, C 5529, D 5504), suggesting that it represents much better the average structure in the study region. This is also reflected in the distribution of Fig. 6d where the number of defining onsets per solution is considered.

Figure 6f provides the distribution of the differences in kilometers between the event epicenters obtained with BAREY, which are used here as reference locations, and the three runs, B, C, and D, with the new average 1-D model, BARENTS16. It is probably not surprising that the results closest to the reference are those of BARENTS16 with all resolvable station corrections; they are calculated to strongly reflect this particular dataset, the velocity model describing an average crust and upper mantle structure, and the station corrections incorporating the deviations from this average.

However, in terms of event location quality, the use of station corrections does not contribute to either the stability or the accuracy of the results. It is always the use of the obtained average model without any corrections applied that exhibits the best uncertainty metrics and fits most of the available data into acceptable solutions. We thereby suggest that under such extreme conditions as in the present application, the velocity average obtained through VELEST is usable, but the station corrections do not have practical value, even when resolvable.

Finally, Figs. 7 and 8 show the overall uncertainties for the relocation scheme with model BARENTS16 without station corrections (B), as well as the shift of the corresponding epicenters from the solution obtained using BAREY (A). Most events in Finnmark, along the SFZ and the sedimentary wedge west and south of

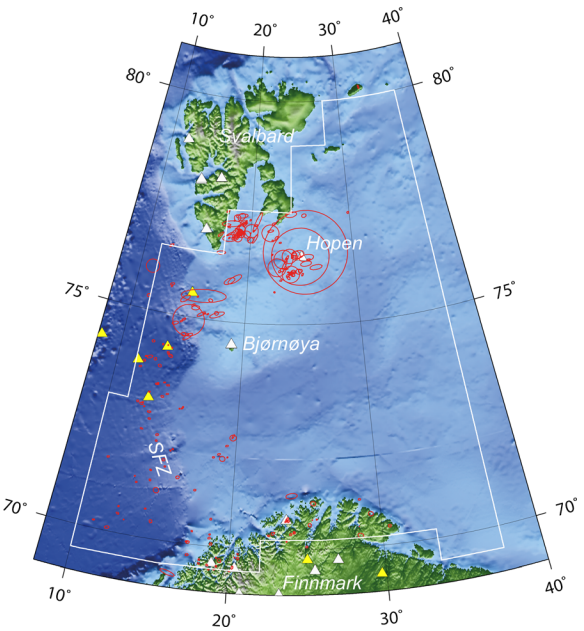

Fig. 7 Ninety-five percent confidence level error ellipses (red) for the 245 events relocated using model BARENTS16 without station corrections. The study region is enclosed in the white polygon, and permanent and temporary stations providing data are denoted as white and yellow triangles, respectively

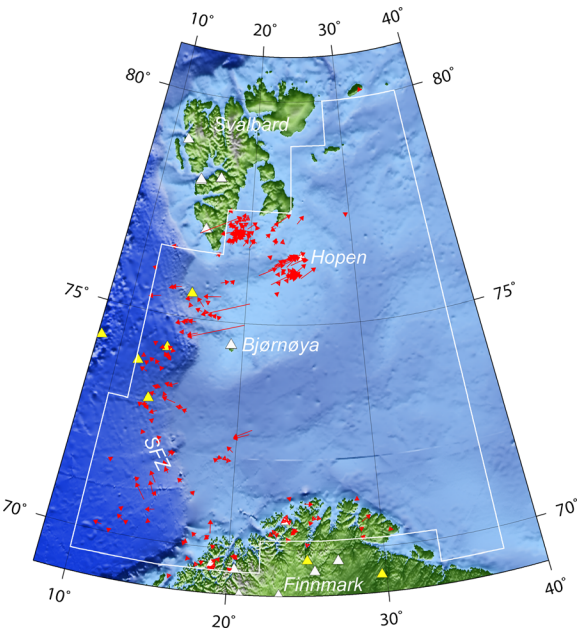

Fig. 8 Vectors (red) showing the epicenter shift between the relocated estimates with BAREY (vector start) and BARENTS16 without station corrections (arrowhead). The study region is enclosed in the white polygon, and permanent and temporary stations providing data are denoted as white and yellow triangles, respectively

Bjørnøya exhibit small error ellipses (Fig. 7); the same applies to most events in the small group in the southwestern Barents Sea. Ellipses increase in size moving northwards; the largest ones are found in the area of Hopen and at the sedimentary wedge northwest of Bjørnøya. Their often elongated shapes, with major axis in a general E–W trend, reflect the absence of stations along the same direction, resulting in poorly constrained location estimates. It is among this population that outliers to the epicenter shift tests for the obtained velocity models are found (see Sect. 3.1), typically involving one station on Svalbard and a few in Fennoscandia.

This problematic is reflected also in the differences between relocation results with different models (Fig. 8). Larger vectors are observed mainly in the area west of Hopen and at Svalbard, as well as north of Bjørnøya, where very few stations were routinely used for event location prior to 2008 (e.g., Pirli et al. 2013).

4 Conclusions

An average 1-D seismic velocity model was calculated for the crust and upper mantle in the western Barents Sea region. The implementation was based on the compilation of a joint seismic bulletin tailored to the study region, combining all available resources. Even so, the sparse recording network and the distances of the stations from the targeted seismicity do not provide high resolution for event location estimates and cannot resolve the focal depth.

In the obtained model, BARENTS16, a simple crustal geometry with two layers is described due to the limited resolution achieved by the employed dataset, with velocities representing the mean of the range of values observed in the region (e.g., based on the crustal part of Barents3D). The Moho is also in good agreement with average depths found in literature.

BARENTS16 will be used primarily for routine event location, replacing the models that were in use until now (e.g., BAREY), which, although performing reasonably, did not reflect the mean Earth structure in the region.

This application has demonstrated that it is possible to obtain a stable velocity average for seismic event location purposes, even with an unfavorable distribution of stations and seismicity, spread over very diverse media in terms of Earth structure, but it is important to understand the implications that this geometry has for the validity of station corrections. We find that although well-resolved station corrections incorporate in a valid manner the part of the heterogeneous velocity structure that cannot be modeled using the current approach, they do not contribute to the improvement of event location results.

Acknowledgements Steven Gibbons provided phase readings for a collection of seismic events in northern Norway, as well as phase readings from stations on Greenland for events in the European Arctic that were relocated within an AFRL contract. Ilma Janutyté provided phase readings from events in Finnmark from temporary deployments realized within the international initiative ScanArray (Thybo et al. 2012). The Arkhangelsk seismic bulletin was provided by Yana Konechnaya and readings from the KRSC station AMD by Andrey Fedorov, within the GEOPROC project co-financed by the Research Council of Norway (project no. 233973) and the Russian Foundation for Basic Research (project no. 14-05-93080). Maps were constructed using the Generic Mapping Tools software (e.g., Wessel and Smith 1998). Bathymetry in Figs. 1a, b, 7, and 8 is shown using the IBCAO grid (Jakobsson et al. 2012), and the mid-ocean ridge system in Figs. 1c and 5a, b is traced using the plate boundaries of Bird (2003). The manuscript benefited from the comments of two anonymous reviewers.

Funding information This research was financed by Aker BP ASA.

References

Bird P (2003) An updated digital model of plate boundaries. Geochem Geophys Geosyst. https://doi.org/10.1029/2001GC000252

Czuba W, Grad M, Mjelde R, Guterch A, Libak A, Krüger F, Murai Y, Schweitzer J, IPY Project Group (2011) Continent-ocean transition across a trans-tensional margin segment: off Bear Island, Barents Sea. Geophys J Int 184:541–554. https://doi.org/10.1111/j.1365-246X.2010.04873.x

Eken T, Shomali ZH, Roberts R, Bödvarsson R (2007) Upper mantle structure of the Baltic Shield below the Swedish National Seismological Network (SNSN) resolved by teleseismic tomography. Geophys J Int 169:617–630. https://doi.org/10.1111/j.1365-246X.2007.03351.x

Eken T, Shomali ZH, Roberts R, Hieronymus CF, Bodvarsson R (2008) S and P velocity heterogeneities within the upper mantle below the Baltic Shield. Tectonophysics 462:109–124. https://doi.org/10.1016/j.tecto.2008.02.015

Grad M, Tiira T, ESC Working Group (2009) The Moho depth map of the European plate. Geophys J Int 176:279–292. https://doi.org/10.1111/j.1365-246X.2008.03919.x

Haslinger F (1998) Velocity structure, seismicity and seismotectonics of Northwestern Greece between the Gulf of Arta and Zakynthos. Dissertation, Swiss Federal Institute of Technology Zürich

Hauser J, Dyer KM, Pasyanos ME, Bungum H, Faleide JI, Clarck SA, Schweitzer J (2011) A probabilistic seismic model for

the European Arctic. J Geophys Res 116:B01303. https://doi.org/10.1029/2010JB007889

Havskov J, Bormann P, Schweitzer J (2012) IS11.1: seismic source location. In: Bormann P (ed) New Manual of Seismological Observatory Practice 2 (NMSOP-2), IASPEI. GFZ German Research Centre for Geosciences, Potsdam, pp 1–80. https://doi.org/10.2312/GFZ.NMSOP-2_IS_11.1

Hejrani B, Balling N, Jacobsen BH, England R (2017) Upper-mantle velocities below the Scandinavian Mountains from P- and S-wave traveltime tomography. Geophys J Int 208:177–192. https://doi.org/10.1093/gji/ggw370

Hicks E, Kværna T, Mykkeltveit S, Schweitzer J, Ringdal F (2004) Travel-times and attenuation relations for regional phases in the Barents Sea region. Pure Appl Geophys 161:1–19

International Seismological Centre (2014) On-line bulletin, http://www.isc.ac.uk, Internatl. Seismol. Cent., Thatcham, United Kingdom. Accessed 17 August 2017

Jakobsson M, Mayer LA, Coakley B, Dowdeswell JA, Forbes S, Fridman B, Hodnesdal H, Noormets R, Pedersen R, Rebesco M, Schenke H-W, Zarayskaya Y, Accettella D, Armstrong A, Anderson RM, Bienhoff P, Camerlenghi A, Church I, Edwards M, Gardner JV, Hall JK, Hell B, Hestvik OB, Kristoffersen Y, Marcussen C, Mohammad R, Mosher D, Nghiem SV, Pedrosa MT, Travaglini PG, Weatherall P (2012) The International Bathymetric Chart of the Arctic Ocean (IBCAO) version 3.0. Geophys Res Lett. https://doi.org/10.1029/2012GL052219

Junek WN, Kværna T, Pirli M, Schweitzer J, Harris DB, Dodge DA, Woods MT (2014) Inferring aftershock sequence properties and tectonic structure using empirical signal detectors. Pure Appl Geophys. https://doi.org/10.1007/s00024-014-0938-0

Kennett BLN, Engdahl ER, Buland R (1995) Constraints on seismic velocities in the Earth from travel times. Geophys J Int 122:108–124

Kissling E (1988) Geotomography with local earthquake data. Rev Geophys 26:659–698

Kissling E (1995) Program VELEST user's guide—short introduction, Institute of Geophysics, ETH Zürich, http://www.seg.ethz.ch/software/velest.html. Accessed 17 August 2017

Kissling E, Ellsworth WL, Eberhart-Phillips D, Kradolfer U (1994) Initial reference models in earthquake tomography. J Geophys Res 99(B10):19635–19646

Klitzke P, Faleide JI, Scheck-Wenderoth M, Sippel J (2015) A lithosphere-scale structural model of the Barents Sea and Kara Sea region. Solid Earth 6:153–172. https://doi.org/10.5194/se-6-153-2015

Levshin A, Schweitzer J, Weidle C, Shapiro N, Ritzwoller M (2007) Surface wave tomography of the Barents Sea and surrounding regions. Geophys J Int 170:441–459

Morozov AN, Vaganova NV, Konechnaya YV, Asming VE (2015) New data about seismicity and crustal velocity structure of the "continent-ocean" transition zone of the Barents-Kara region in the Arctic. J Seismol 19(1):219–230. https://doi.org/10.1007/s10950-014-9462-z

Müller G (1977) Earth flattening approximation for body waves derived from geometric ray theory—improvements, corrections and range of applicability. J Geophys 42:429–436

Mykkeltveit S, Ringdal F (1981) Phase identification and event location at regional distance using small-aperture array data. In: Husebye ES, Mykkeltveit S (eds) Identification of seismic sources—earthquake or underground explosion, NATO Advanced Study Institutes Series (Series C – Mathematical and Physical Sciences), vol 74. Springer, Dordrecht, pp 467–481. https://doi.org/10.1007/978-94-009-8531-5_23

Pirli M, Schweitzer J, Ottemöller L, Raeesi M, Mjelde R, Atakan K, Guterch A, Gibbons SJ, Paulsen B, Dębski W, Wiejacz P, Kværna T (2010) Preliminary analysis of the 21 February 2008, Svalbard (Norway), seismic sequence. Seismol Res Lett 81:63–75

Pirli M, Schweitzer J, the IPY Project Consortium (2011) The International Polar Year (IPY) broadband ocean-bottom seismograph deployment: observations, limitations and integration with the IPY land network. NORSAR Sci Rep 2-2011:51–64

Pirli M, Schweitzer J, Paulsen B (2013) The Storfjorden, Svalbard, 2008-2012 aftershock sequence: seismotectonics in a polar environment. Tectonophysics 601:192–205. https://doi.org/10.1016/j.tecto.2013.05.010

Ritzmann O, Maercklin N, Faleide JI, Bungum H, Mooney WD, Detweiler ST (2007) A 3D geophysical model for the crust in the greater Barents Sea region: database compilation, model construction and basement characterization. Geophys J Int 170:417–435

Schweitzer J (2001) HYPOSAT—an enhanced routine to locate seismic events. Pure Appl Geophys 158:277–289

Schweitzer J (2011) The dynamic continental margin between the Mid-Atlantic Ridge and Bjørnøya (Bear Island). In: Orheim O, Ulstein K (eds) The Norwegian Contribution (International Polar Year 2007-2008). The Research Council of Norway, Oslo, pp 168–172 ISBN:978-82-12-02901-9

Schweitzer J, Kennett BLN (2007) Comparison of location procedures: the Kara Sea event of 16 August 1997. Bull Seismol Soc Am 97:389–400

Schweitzer J, Antonovskaya G, Joint Norwegian-Russian Project GEOPROC Consortium (2017) The project "Seismological research related to geophysical processes in the European Arctic (GEOPROC)" and "Recommendations for future Norwegian-Russian geophysical cooperation in the European Arctic". NORSAR Annual Sci Rep 2016 (in print)

Silvennoinen H, Kozlovskaya E, Kissling E, Kosarev G, the POLENET/LAPNET Working Group (2014) A new Moho boundary map for the northern Fennoscandian Shield based on combined controlled-source seismic and receiver function data. Geo Res J 1-2:19–32. https://doi.org/10.1016/j.grj.2014.03.001

Smelror M, Petrov OV, Larssen GB, Werner SC (2009) ATLAS. Geological history of the Barents Sea. Geological Survey of Norway, Trondheim, https://issuu.com/ngu_/docs/atlas_-_geological_history_of_the_b/1?e=3609664/9026048/ . Accessed 17 August 2017

Stange S, Schweitzer J (2004) Source depths at regional distances: an example from the western Barents Sea/Svalbard region. NORSAR Sci Rep 1-2004:45–50

Thybo H, Balling N, Maupin V, Ritter J, Tilmann F (2012) ScanArray Core (1G 2012-2017). The ScanArray consortium. Other/Seism Netw. https://doi.org/10.14470/6T569239

Tukey JW (1977) Exploratory data analysis. Addison-Wesley Publishing Company, Reading, pp xvi+688

Wessel P, Smith WHF (1998) New, improved version of Generic Mapping Tools released. EOS Trans Am Geophys Union 79(47):579

Wilde-Piórko M (2015) Crustal and upper mantle seismic structure of the Svalbard Archipelago from the receiver function analysis. Polish Polar Res 36:89–107. https://doi.org/10.1515/popore-2015-0009